

Nanosecond solvation dynamics in a polymer electrolyte for lithium batteries

Received: 20 October 2023

Accepted: 6 February 2024

Published online: 27 February 2024

 Check for updates

Neel J. Shah ^{1,2,5}, Chao Fang ^{1,2,5}, Naresh C. Osti ³, Eugene Mamontov ³, Xiaopeng Yu², Jaeyong Lee ², Hiroshi Watanabe⁴, Rui Wang ^{1,2}  & Nitash P. Balsara ^{1,2} 

Solvation dynamics critically affect charge transport. Spectroscopic experiments and computer simulations show that these dynamics in aqueous systems occur on a picosecond timescale. In the case of organic electrolytes, however, conflicting values ranging from 1 to several 100 picoseconds have been reported. We resolve this conflict by studying mixtures of an organic polymer and a lithium salt. Lithium ions coordinate with multiple polymer chains, resulting in temporary crosslinks. Relaxation of these crosslinks, detected by quasielastic neutron scattering, are directly related to solvation dynamics. Simulations reveal a broad spectrum of relaxation times. The average timescale for solvation dynamics in both experiment and simulation is one nanosecond. We present the direct measurement of ultraslow dynamics of solvation shell break-up in an electrolyte.

Ion transport and reaction rates in electrolytes are governed by the relaxation rate of the molecules surrounding the ions^{1–3}. The term ‘solvation’ generally applies to the immediate neighbourhood of an ion in a dilute liquid electrolyte; in this limit, the neighbourhood is dominated by solvent molecules, hence the term solvation. It has long been recognized that these environments are dynamic in nature due to both inertial effects and translation of the solvent molecules away from the solvation shell. The structure of solvation shells can be studied by a variety of experiments^{4–8} including vibrational spectroscopy⁹, nuclear magnetic resonance¹⁰ and X-ray scattering¹¹. Confidence in our understanding of the structure of solvation shells is bolstered by the agreement between molecular dynamics (MD) simulations and experiments^{12–14}. The break-up of solvation shells occurs due to a collection of relaxation modes, and we use the term ‘lifetime’ to quantify the characteristic timescale of the dominant modes. In the case of aqueous electrolytes, both experiments and theory confirm that this timescale is in the 1–10 ps range^{15–19}. However, the timescale for the motion of organic molecules in the vicinity of ions remains under debate. Using two-dimensional infrared spectroscopy, picosecond spectral dynamics have been observed in many organic electrolytes^{20–28},

which is interpreted as a chemical exchange of solvent molecules surrounding a mobile cation. Corroborated by MD simulations of spectral dynamics, the features in two-dimensional infrared spectroscopy were attributed to the timescale of solvation. By contrast, Dereka et al. recently used two-dimensional infrared spectroscopy to study a broad selection of cations in acetonitrile and demonstrated that the spectral dynamics of two-dimensional infrared spectroscopy are solely a result of intermolecular vibrational energy transfer²⁹. The lower boundary of solvation lifetime is instead several hundred picoseconds. This conclusion is also supported by MD simulations that directly quantify the solvent exchange time^{29–31}.

Lithium salts dissolved in organic solvents have received considerable interest due to their relevance in rechargeable lithium batteries, wherein the rate at which these batteries can be charged and discharged depends directly on the solvation timescale. In addition to liquid electrolytes, there is considerable interest in both inorganic and polymeric electrolytes, as they may enable fundamentally different battery chemistries with higher energy densities and improved safety³². The purpose of this study is to present a new approach for measuring solvation dynamics in a polymer electrolyte based on quasielastic

¹Department of Chemical and Biomolecular Engineering, University of California, Berkeley, CA, USA. ²Materials Sciences Division, Lawrence Berkeley National Laboratory, Berkeley, CA, USA. ³Neutron Scattering Division, Oak Ridge National Laboratory, Oak Ridge, TN, USA. ⁴Institute for Chemical Research, Kyoto University, Uji, Japan. ⁵These authors contributed equally: Neel J. Shah, Chao Fang.  e-mail: ruiwang325@berkeley.edu; nbalsara@berkeley.edu

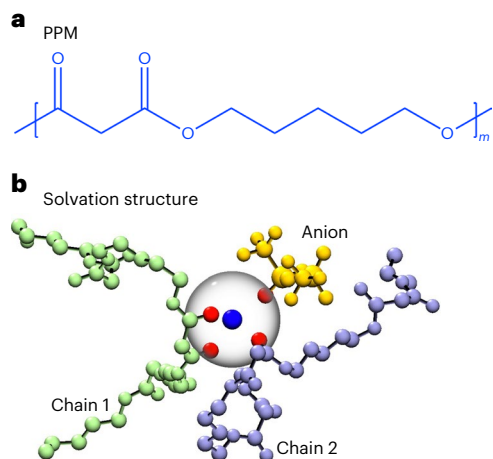


Fig. 1 | PPM polymer and Li⁺ solvation structure. **a**, Chemical structure of PPM polymer. **b**, Typical solvation structure of Li⁺ in PPM represented by the ball-and-stick model. Li⁺ is shown as a blue sphere, the solvation cage is shown as a large transparent sphere and oxygen atoms within the cage are shown in red.

neutron scattering (QENS). When considered in conjunction with computer simulations, our results demonstrate that the timescale for motion of the polymer segments in the neighbourhood of a lithium ion is on the order of 1 ns, a timescale ideally suited for QENS. This is a direct measurement of ultraslow dynamics of solvation shell break-up. We use our validated computer simulations to estimate the solvation timescale as a function of chain length down to the small molecule limit. We obtain a value of 0.22 ns, consistent with the lower bound presented in the literature²⁹.

Our electrolyte is a mixture of a lithium salt, lithium bis(trifluoromethanesulfonyl)imide (LiTFSI), and a polymer, poly(pentyl malonate) (PPM), shown in Fig. 1a. The electrochemical properties of this electrolyte are summarized in Supplementary Section 4. The dominant solvation environment of lithium ions comprises oxygen atoms from two different PPM chains (and an anion)³³, as shown in Fig. 1b. One may view the lithium ion as a crosslink that temporarily binds two polymer chains together. In other words, the lithium ions create reversible crosslinks within the electrolyte. It is natural to conclude that the formation and breakage of the lithium solvation structure, that is, the solvation dynamics, are identical to the crosslink dynamics. The dynamics of polymer chains in the presence of temporary crosslinks is a subject of continuing interest^{34–38}, mainly due to their effect on the rheological properties of associating polymers, vitrimers and physical gels. Models that describe this motion serve as a foundation for interpreting the simulations and QENS data obtained from our polymer electrolyte.

Our experimental approach rests on the determination of the time dependence (t) of the mean-squared displacement ($\langle r_d^2(t) \rangle$) of the polymer segments by QENS on segmental (10 Å) length scales^{39,40}. In the absence of temporary crosslinks, the motion of polymer chains on the segmental length scales is governed by the Rouse model^{41–43}, which obtains $\langle r_d^2(t) \rangle \propto t^{1/2}$. At high enough salt concentrations, we obtain signatures corresponding to the 'sticky' Rouse model. We use MD simulations to interpret the QENS data and elucidate the relationship between the segmental dynamics and the lifetime of the solvation structure.

QENS is ideally suited for measuring motion induced by thermal fluctuations because the energy of neutrons is comparable to the thermal energy kT (k is the Boltzmann constant and T is temperature), which is in the millielectronvolt range. The large incoherent scattering cross-section of hydrogen dominates the signal from these experiments, allowing QENS to capture the motion of PPM segments with many hydrogen atoms. To obtain these measurements, we used the

Backscattering Spectrometer at the Spallation Neutron Source at Oak Ridge National Laboratory⁴⁴. We collected data at 363 K and 30 K. The latter dataset was used to determine the instrument resolution function. To a good approximation, the magnitude of the scattering vector, Q , is given by $Q = 4\pi \sin(\theta/2)/\lambda_i$, where θ is the scattering angle and λ_i is the wavelength of the incident neutrons (Supplementary Section 6 for details). The narrow resolution function of our instrument enables the detection of energy changes of the scattered neutrons, E , in the microelectronvolt range, and the accessible Q window is commensurate with the length scale of PPM segments (Fig. 1). In Fig. 2a, we plot the incoherent structure factor $S_{\text{inc}}(Q, \omega)$ as a function of energy transfer $E = (\hbar/2\pi)\omega$ obtained from a series of PPM/LiTFSI mixtures, where \hbar is Planck's constant and ω is the angular frequency. The concentration of the electrolytes is specified by r , the molar ratio of lithium ions to oxygen atoms from PPM chains. This measure of concentration is convenient as it provides a measure of the ratio of lithium ions to polymer segments (each segment contains four oxygen atoms). In Fig. 2a, we see a characteristic narrowing of the QENS spectra as a function of salt concentration, indicative of a slowdown in segmental dynamics as a function of added salt.

Analysis of the QENS data is facilitated by transforming $S_{\text{inc}}(Q, \omega)$ into the time domain. We accomplished this using Mantid (v.51), a program provided by Oak Ridge National Laboratory⁴⁵. In Fig. 2b, we show $S_{\text{inc}}(t)$ on a semi-log plot. A simple decay is observed in the salt-free sample and in electrolytes with $r < 0.04$. However, a new feature emerges in electrolytes with $r \geq 0.04$ at timescales larger than 0.4 ns. The connection between QENS and solvation dynamics was enabled by the serendipitous discovery of this new feature.

In the limit of sufficiently small Q , the time dependence of the mean-squared displacement of polymer segments, $\langle r_d^2(t) \rangle$, can be determined from the transformation of $S_{\text{inc}}(Q, \omega)$ in the time domain:

$$S_{\text{inc}}(Q, t) = \exp\left[\frac{-Q^2}{6} \langle r_d^2(t) \rangle\right]. \quad (1)$$

The accuracy of this approximation decreases with increasing Q , hence our choice of a low $Q = 0.5 \text{ \AA}^{-1}$ for data analysis.

In the subdiffusive regime, the motion of polymer segments is governed by Rouse dynamics^{41–43} and $\langle r_d^2 \rangle$ is proportional to $t^{1/2}$. To focus on the subdiffusive processes in PPM, we examine the Rouse parameter, which we define as $\langle r_d^2 \rangle / t^{1/2}$, as a function of t (Fig. 3a). In a salt-free system ($r = 0$), the Rouse parameter is more or less consistent with the standard Rouse model describing the motion of polymer chains^{41–43}. In the 0.25 to 0.60 ns time window, the Rouse parameter shows a plateau as expected, and it increases at longer times as the crossover from the subdiffusive to the diffusive regime begins. The diffusive regime, which we estimate to be observed on timescales of 5,000 ns, is well outside our experimental window (Supplementary Section 12). At early times ($t \leq 0.25$ ns), the measured Rouse parameter increases with time, a feature that is not consistent with the Rouse model. It appears that the $\langle r_d^2 \rangle$ versus t scaling exponent at very early times is larger than that predicted by the Rouse model. We are unable to provide a definitive explanation for the very early time observations. As salt concentration increases beyond $r = 0.04$, the Rouse parameter in the $t > 0.25$ ns regime deviates notably from the standard Rouse model. In this regime, we observe a decrease of $\langle r_d^2 \rangle / t^{1/2}$ followed by a plateau, which is seen clearly at $r = 0.10$ (marked as P_1) and then a subsequent increase. The reduction of the Rouse parameter in PPM at high salt concentration resembles the effect of temporary crosslinks on chain dynamics in associating polymers, as described by the 'sticky Rouse model'^{34,35,46}. In this model, the $\langle r_d^2 \rangle \propto t^{1/2}$ regime gives way to a new regime wherein $\langle r_d^2 \rangle \propto t^{1/4}$ due to the slowing of polymer segments as they interact with the stickers. This results in a suppressed plateau that reflects sticker-segment interactions. On timescales much larger than the sticker lifetime, the $\langle r_d^2 \rangle$ versus t scaling exponent increases due to a crossover

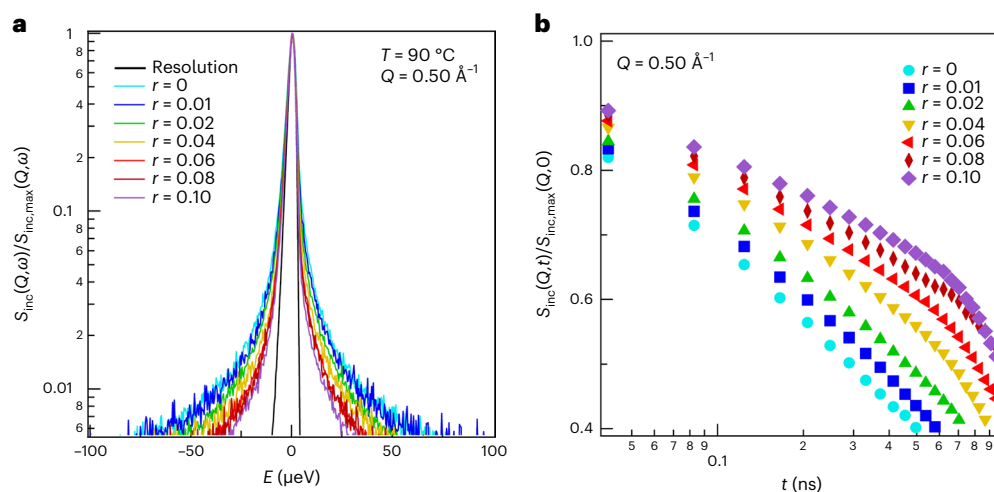


Fig. 2 | Structure factors obtained by QENS. a, Normalized incoherent structure factor $S_{\text{inc}}(Q, \omega)/S_{\text{inc,max}}(Q, \omega)$ ($S_{\text{inc,max}}(Q, \omega)$ is the maximum of the structure factor), in the frequency domain, plotted as a function of incident energy of the neutrons, E , at $Q = 0.50 \text{ \AA}^{-1}$ and 363 K. **b**, Corresponding structure factor in the time domain.

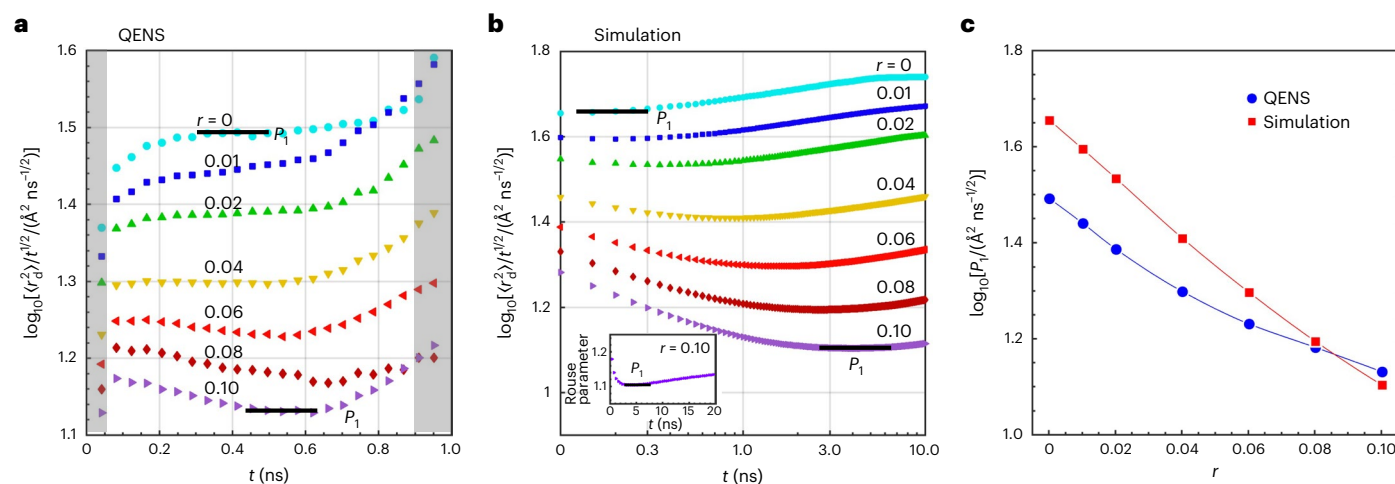


Fig. 3 | Segmental dynamics determined by QENS and simulation.

a, b, Evolution of the Rouse parameter $\langle r_d^2 \rangle / t^{1/2}$ as a function of time t in QENS (**a**) and MD simulation (**b**). The grey shaded regions in **a** denote regimes with substantial uncertainty due to proximity to the high and low energy transfer

boundaries of the QENS instrument. P_1 in **a** and **b** marks the plateau value.

The inset in **b** shows the Rouse parameter on a linear timescale for $r = 0.10$.

c, Comparison of plateau values obtained by QENS and simulation as a function of salt concentration r .

to the diffusive regime. In our system, the temporary crosslinks are created because the solvation structure surrounding Li^+ ions comprises segments belonging to different chains, as depicted in Fig. 1b.

We next employ MD simulations to elucidate the underlying mechanisms of the observed temporary crosslinks. MD simulations were performed in the NpT (constant pressure p ; constant temperature T ; constant particle number N) ensemble based on the all-atom optimized potentials for liquid simulations (OPLS-AA) force field (Supplementary Section 7 for details). The segmental motion of polymer chains was analysed by calculating the mean-squared displacement of hydrogen atoms on the chains, as they dominate the QENS signal due to their large incoherent scattering cross-section⁴⁷. Figure 3b depicts the computed Rouse parameter as a function of time. Qualitatively similar signatures of QENS are observed in simulation, including the dynamics of free chains in a salt-free system and signatures related to the presence of temporary crosslinks at high salt concentrations ($r \geq 0.04$). The simulation results also capture the evolution of the plateau values (P_1) as salt concentration increases. While the absolute values of P_1 obtained in experiments and simulations are not in perfect agreement, their dependence on salt concentration

is similar. This is shown in Fig. 3c, where P_1 values obtained by QENS and simulation are plotted as a function of salt concentration. The maximum difference between theory and experiment is about 10%. However, the timescales of the plateau regimes, which signify the presence of temporary crosslinks, are larger in the simulation compared to the experimental observations. This discrepancy could be attributed to the limitations of the atomic models used in the simulation, which do not account for factors such as polarizability. There is also a lack of agreement between theory and experiment at very short times ($t \leq 0.2$ ns). Neither the Rouse theory nor the MD simulations provide a reason for the observed dynamics at very short times. Overall, the simulations are consistent with many of the key experimental observations.

The lifetimes of temporary crosslinks can be precisely quantified in simulation owing to the high resolution of $\langle r_d^2(t) \rangle$ data as a function of time. Figure 4a illustrates the determination of two characteristic times, denoted as τ_1 and τ_2 , at a salt concentration of $r = 0.10$. τ_1 represents the timescale at which the plateau regime begins, while τ_2 indicates the completion of the plateau regime and the subsequent increase in Rouse parameter. We determined τ_1 and τ_2 at all salt concentrations,

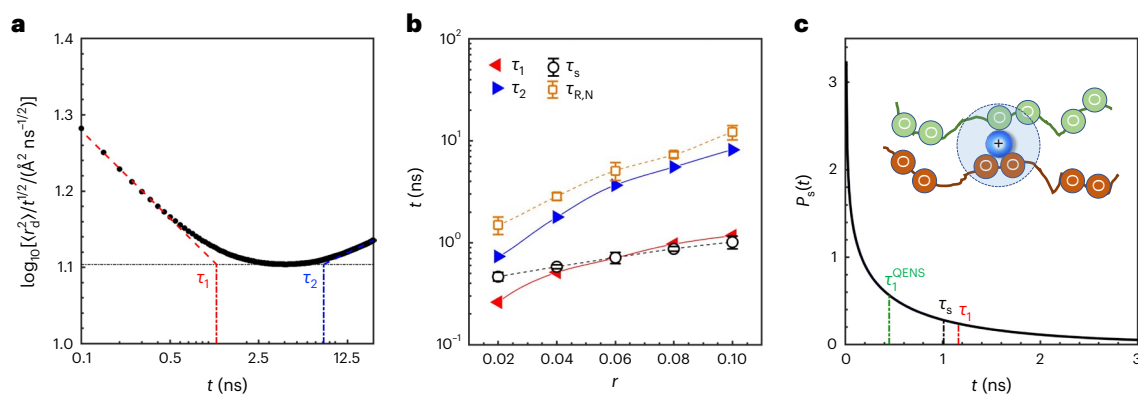


Fig. 4 | Solvation dynamics in the presence of temporary Li⁺ crosslinks.

a, A plot of the Rouse parameter ($\langle r_d^2 \rangle / t^{1/2}$) as a function of time obtained by simulation at a salt concentration of $r = 0.1$. Timescales τ_1 and τ_2 are defined as the intersection between the two fitted lines and the plateau (the horizontal dashed line). **b**, Comparison of different timescales as a function of salt concentration, r ; τ_s is the average lifetime of the solvation structure, and $\tau_{R,N}$ is the fastest Rouse relaxation time of the PPM chains. Data are presented as mean values from four independent simulations and error bars denote the standard deviation.

c, Probability distribution of the lifetime of the solvation structure at $r = 0.10$. The inset shows the schematic illustration of the solvation structure surrounding the Li⁺ ion that acts as a crosslink. The lifetime is defined as the duration of one monomer that stays within a given crosslink. The timescales at $r = 0.10$ obtained from simulations—the average solvation lifetime (τ_s), and that at the start of the Rouse plateau (τ_1)—are compared with the experimentally measured time at the start of the Rouse plateau (τ_1^{QENS}).

as depicted in Fig. 4b. Both τ_1 and τ_2 increase monotonically with increasing salt concentration.

The characteristic times identified above are related to dynamic processes occurring on the segmental level. The formation of a temporary solvation cage structure slows the motion of associated segments. Each solvation cage consists of oxygens from different chains. A monomer is considered to be within the solvation cage when it provides at least one carbonyl oxygen atom to coordinate the cation (as illustrated in the inset of Fig. 4c). The time required for the oxygens to desolvate is thus determined. A typical probability distribution of lifetimes, defined as $P_s(t)$, is depicted in Fig. 4c, where we have used a salt concentration of $r = 0.10$. While the distribution is broad, as is the case in the well-studied system of aqueous electrolytes^{29,31}, and the lifetime can approach several nanoseconds, the majority of monomers remain in a given solvation structure for a timescale of about 1 ns. The average lifetime of monomers in the solvation cage is extracted from the probability distribution as

$$\tau_s = \int_0^{\infty} P_s(t) dt. \quad (2)$$

At $r = 0.10$, τ_s is very close to τ_1 , as illustrated by the two dashed lines in Fig. 4c. This agreement between τ_s and τ_1 holds for different salt concentrations, as shown in Fig. 4b; τ_1 can thus be interpreted as the characteristic solvation lifetime. A longer solvation lifetime is expected in polymer electrolytes compared to that in small organic solvents. We conducted simulations as a function of the chain length of PPM as shown in Supplementary Fig. 5. Our estimate for the solvation lifetime for a monomer of PPM is 0.2 ns, consistent with the ‘ultraslow’ lower bound of 0.1 ns proposed by Dereka et al.²⁹. The ionic conductivity of aqueous electrolytes such as NaCl in water at room temperature can approach values as high as 200 mS cm⁻¹ (ref. 48), a value that is 20-fold higher than that of the optimized lithium battery electrolyte, 10 mS cm⁻¹ (ref. 49). It is likely that an important underlying factor is the difference in solvation lifetimes (10 versus 200 ps). We have compared the solvation timescales of aqueous electrolytes at room temperature with those of non-aqueous electrolytes at 90 °C. While further work is needed to compare the timescales at the same temperature, there is little doubt that the solvation dynamics are certainly faster at higher temperatures. This makes the ultraslow process we have studied in the non-aqueous electrolyte even slower (Supplementary Fig. 6).

Beyond τ_1 , the association between segments and Li⁺ becomes less important, leading to the plateau regime observed in the Rouse parameter. The termination of the plateau regime, which is marked by τ_2 , represents the onset of the transition of the segmental motion from the subdiffusive regime to the diffusive regime. This is demonstrated in Fig. 4b, wherein τ_2 is close to but smaller than $\tau_{R,N}$ at all salt concentrations. Here, $\tau_{R,N}$ represents the fastest Rouse relaxation time, specifically the relaxation time of individual segments, obtained through Rouse mode analysis (subscripts R and N respectively denote Rouse relaxation and the mode number; details in Supplementary Section 12). In our analysis, $\tau_{R,N}$ reflects the effective relaxation times that are averaged from both non-sticky and sticky segments.

While further work is needed to establish the extent to which the observed signatures of τ_1 and τ_2 are general, we expect the reported signatures to be found in any polymer electrolyte wherein the solvating groups are donated by different polymer chains. This is likely to be the case for most polymer electrolytes. One exception to this is the well-studied polymer electrolyte poly(ethylene oxide) mixed with LiTFSI, which has ether oxygens along the chain at distances that are very similar to crown ethers. Due to this, the dominant solvation structure in poly(ethylene oxide)/LiTFSI comprises ether oxygens from one chain^{33,50}. Generally speaking, the efficacy of an electrolyte in practical applications depends on continuum ion transport properties (conductivity, diffusion coefficient and transference number). Qualitatively, we expect that decreasing solvation lifetimes leads to faster continuum transport of lithium ions. Our work thus suggests that improved electrolytes may be designed by rapid screening of electrolytic systems using solvation lifetime.

In conclusion, we have combined QENS and MD simulations to study the dynamics of polymer segments in the vicinity of coordinating Li⁺ ions. QENS measurements revealed that the time-dependent mean-squared displacement follows the standard Rouse model in a salt-free system. However, substantial deviations from the Rouse model, characterized by a decrease in the Rouse parameter followed by a plateau, were observed as salt concentration increases. These are signatures of temporary crosslinks that are formed because Li⁺ ions typically coordinate with segments from more than one chain. Simulations show that timescales related to the temporary-crosslink plateau are nearly identical to the solvation lifetime. Both experiments and simulations indicate that this lifetime is on the order of 1 ns in PPM/LiTFSI, providing direct measurement of ultraslow dynamics of solvation shell break-up in an electrolyte.

Online content

Any methods, additional references, Nature Portfolio reporting summaries, source data, extended data, supplementary information, acknowledgements, peer review information; details of author contributions and competing interests; and statements of data and code availability are available at <https://doi.org/10.1038/s41563-024-01834-y>.

References

1. Wolyne, P. G. Dynamics of electrolyte solutions. *Annu. Rev. Phys. Chem.* **31**, 345–376 (1980).
2. Ratner, M. A., Johansson, P. & Shriver, D. F. Polymer electrolytes: ionic transport mechanisms and relaxation coupling. *MRS Bull.* **25**, 31–37 (2000).
3. Marcus, R. A. On the theory of oxidation-reduction reactions involving electron transfer. I. *J. Chem. Phys.* **24**, 966–978 (1956).
4. Bakker, H. Structural dynamics of aqueous salt solutions. *Chem. Rev.* **108**, 1456–1473 (2008).
5. Bagchi, B. & Jana, B. Solvation dynamics in dipolar liquids. *Chem. Soc. Rev.* **39**, 1936–1954 (2010).
6. Ohtaki, H. & Radnai, T. Structure and dynamics of hydrated ions. *Chem. Rev.* **93**, 1157–1204 (1993).
7. He, F. & Richert, R. Solvation dynamics in viscous polymer solution: propylene carbonate confined by poly(methylmethacrylate). *Phys. Rev. B* **74**, 014201 (2006).
8. Zhang, X.-X., Liang, M., Ernsting, N. P. & Maroncelli, M. Complete solvation response of coumarin 153 in ionic liquids. *J. Phys. Chem. B* **117**, 4291–4304 (2013).
9. Ben-Amotz, D. Hydration-shell vibrational spectroscopy. *J. Am. Chem. Soc.* **141**, 10569–10580 (2019).
10. Sacco, A. Structure and dynamics of electrolyte solutions. A NMR relaxation approach. *Chem. Soc. Rev.* **23**, 129–136 (1994).
11. Pasquarello, A. et al. First solvation shell of the Cu(II) aqua ion: evidence for fivefold coordination. *Science* **291**, 856–859 (2001).
12. Markovich, G., Perera, L., Berkowitz, M. L. & Cheshnovsky, O. The solvation of Cl⁻, Br⁻, and I⁻ in acetonitrile clusters: photoelectron spectroscopy and molecular dynamics simulations. *J. Chem. Phys.* **105**, 2675–2685 (1996).
13. Kuzmin, A., Obst, S. & Purans, J. X-ray absorption spectroscopy and molecular dynamics studies of hydration in aqueous solutions. *J. Phys. Condens. Matter* **9**, 10065 (1997).
14. Laage, D. & Hynes, J. T. Reorientational dynamics of water molecules in anionic hydration shells. *Proc. Natl Acad. Sci. USA* **104**, 11167–11172 (2007).
15. Jimenez, R., Fleming, G. R., Kumar, P. & Maroncelli, M. Femtosecond solvation dynamics of water. *Nature* **369**, 471–473 (1994).
16. Kropman, M. & Bakker, H. Dynamics of water molecules in aqueous solvation shells. *Science* **291**, 2118–2120 (2001).
17. Rey, R. & Hynes, J. T. Solvation dynamics in water. 4. On the initial regime of solvation relaxation. *J. Phys. Chem. B* **124**, 7668–7681 (2020).
18. Lewis, N. H. C., Dereka, B., Zhang, Y., Maginn, E. J. & Tokmakoff, A. From networked to isolated: observing water hydrogen bonds in concentrated electrolytes with two-dimensional infrared spectroscopy. *J. Phys. Chem. B* **126**, 5305–5319 (2022).
19. Kacenauskaitė, L., Van Wyck, S. J., Moncada Cohen, M. & Fayer, M. D. Water-in-salt: fast dynamics, structure, thermodynamics, and bulk properties. *J. Phys. Chem. B* **128**, 291–302 (2024).
20. Lee, K.-K. et al. Ultrafast fluxional exchange dynamics in electrolyte solvation sheath of lithium ion battery. *Nat. Commun.* **8**, 14658 (2017).
21. Liang, C., Kwak, K. & Cho, M. Revealing the solvation structure and dynamics of carbonate electrolytes in lithium-ion batteries by two-dimensional infrared spectrum modeling. *J. Phys. Chem. Lett.* **8**, 5779–5784 (2017).
22. Fulfer, K. D. & Kuroda, D. G. Solvation structure and dynamics of the lithium ion in organic carbonate-based electrolytes: a time-dependent infrared spectroscopy study. *J. Phys. Chem. C* **120**, 24011–24022 (2016).
23. Fulfer, K. D. & Kuroda, D. G. Ion speciation of lithium hexafluorophosphate in dimethyl carbonate solutions: an infrared spectroscopy study. *Phys. Chem. Chem. Phys.* **20**, 22710–22718 (2018).
24. Rushing, J. C., Leonik, F. M. & Kuroda, D. G. Effect of solvation shell structure and composition on ion pair formation: the case study of LiTfI in organic carbonates. *J. Phys. Chem. C* **123**, 25102–25112 (2019).
25. Chen, X., Fulfer, K. D., Woodard, K. T. & Kuroda, D. G. Structure and dynamics of the lithium-ion solvation shell in ureas. *J. Phys. Chem. B* **123**, 9889–9898 (2019).
26. Lim, J. et al. Two-dimensional infrared spectroscopy and molecular dynamics simulation studies of nonaqueous lithium ion battery electrolytes. *J. Phys. Chem. B* **123**, 6651–6663 (2019).
27. Galle Kankanamge, S. R. & Kuroda, D. G. Molecular structure, chemical exchange, and conductivity mechanism of high concentration LiTFSI electrolytes. *J. Phys. Chem. B* **124**, 1965–1977 (2020).
28. Fulfer, K. D., Galle Kankanamge, S. R., Chen, X., Woodard, K. T. & Kuroda, D. G. Elucidating the mechanism behind the infrared spectral features and dynamics observed in the carbonyl stretch region of organic carbonates interacting with lithium ions. *J. Chem. Phys.* **154**, 234504 (2021).
29. Dereka, B. et al. Exchange-mediated transport in battery electrolytes: ultrafast or ultraslow? *J. Am. Chem. Soc.* **144**, 8591–8604 (2022).
30. Ganesh, P., Jiang, D.-E. & Kent, P. Accurate static and dynamic properties of liquid electrolytes for Li-ion batteries from ab initio molecular dynamics. *J. Phys. Chem. B* **115**, 3085–3090 (2011).
31. Zhang, X. & Kuroda, D. G. An ab initio molecular dynamics study of the solvation structure and ultrafast dynamics of lithium salts in organic carbonates: a comparison between linear and cyclic carbonates. *J. Chem. Phys.* **150**, 184501 (2019).
32. Siegel, D. J., Nazar, L., Chiang, Y.-M., Fang, C. & Balsara, N. P. Establishing a unified framework for ion solvation and transport in liquid and solid electrolytes. *Trends Chem.* **3**, 807–818 (2021).
33. Yu, X. et al. A practical polymer electrolyte for lithium and sodium batteries: poly(pentyl malonate). *ACS Energy Lett.* **7**, 3791–3797 (2022).
34. Leibler, L., Rubinstein, M. & Colby, R. H. Dynamics of reversible networks. *Macromolecules* **24**, 4701–4707 (1991).
35. Rubinstein, M. & Semenov, A. N. Thermoreversible gelation in solutions of associating polymers. 2. Linear dynamics. *Macromolecules* **31**, 1386–1397 (1998).
36. Kumar, S. K. & Douglas, J. F. Gelation in physically associating polymer solutions. *Phys. Rev. Lett.* **87**, 188301 (2001).
37. Suzuki, S., Uneyama, T., Inoue, T. & Watanabe, H. Nonlinear rheology of telechelic associative polymer networks: shear thickening and thinning behavior of hydrophobically modified ethoxylated urethane (HEUR) in aqueous solution. *Macromolecules* **45**, 888–898 (2012).
38. Rapp, P. B., Omar, A. K., Silverman, B. R., Wang, Z.-G. & Tirrell, D. A. Mechanisms of diffusion in associative polymer networks: evidence for chain hopping. *J. Am. Chem. Soc.* **140**, 14185–14194 (2018).
39. Sinha, K. & Maranas, J. K. Segmental dynamics and ion association in PEO-based single ion conductors. *Macromolecules* **44**, 5381–5391 (2011).
40. Mongcopa, K. I. S. et al. Relationship between segmental dynamics measured by quasi-elastic neutron scattering and conductivity in polymer electrolytes. *ACS Macro Lett.* **7**, 504–508 (2018).

41. Rouse, P. E. Jr A theory of the linear viscoelastic properties of dilute solutions of coiling polymers. *J. Chem. Phys.* **21**, 1272–1280 (1953).
42. Doi, M. & Edwards S.F. *The Theory of Polymer Dynamics* (Clarendon Press, 1986).
43. Choo, Y., Halat, D. M., Villaluenga, I., Timachova, K. & Balsara, N. P. Diffusion and migration in polymer electrolytes. *Prog. Polym. Sci.* **103**, 101220 (2020).
44. Mamontov, E. & Herwig, K. W. A time-of-flight backscattering spectrometer at the Spallation Neutron Source, BASIS. *Rev. Sci. Instrum.* **82**, 085109 (2011).
45. Arnold, O. et al. Mantid—data analysis and visualization package for neutron scattering and μ SR experiments. *Nucl. Instrum. Methods Phys. Res. A* **764**, 156–166 (2014).
46. Rubinstein, M. & Semenov, A. N. Dynamics of entangled solutions of associating polymers. *Macromolecules* **34**, 1058–1068 (2001).
47. Börner, H. et al. *Neutron Data Booklet* (Institut Laue-Langevin, 2003).
48. Speight, J. *Lange's Handbook of Chemistry* (McGraw-Hill Education, 2005).
49. Xu, K. Nonaqueous liquid electrolytes for lithium-based rechargeable batteries. *Chem. Rev.* **104**, 4303–4418 (2004).
50. Fang, C., Yu, X., Chakraborty, S., Balsara, N. P. & Wang, R. Molecular origin of high cation transference in mixtures of poly(pentyl malonate) and lithium salt. *ACS Macro Lett.* **12**, 612–618 (2023).

Publisher's note Springer Nature remains neutral with regard to jurisdictional claims in published maps and institutional affiliations.

Springer Nature or its licensor (e.g. a society or other partner) holds exclusive rights to this article under a publishing agreement with the author(s) or other rightsholder(s); author self-archiving of the accepted manuscript version of this article is solely governed by the terms of such publishing agreement and applicable law.

© The Author(s), under exclusive licence to Springer Nature Limited 2024

Data availability

The Supplementary Information contains details of QENS and simulation. Further data are available from the corresponding authors upon request. Source data are presented in this paper.

Acknowledgements

This work was supported by the Joint Center for Energy Storage Research (JCESR), an Energy Innovation Hub funded by the US Department of Energy, Office of Science, Office of Basic Energy Science, under contract no. DE-AC02-06CH11357. This research used resources at the Spallation Neutron Source, a US Department of Energy, Office of Science User Facility operated by Oak Ridge National Laboratory. The computations were performed at the Lawrence Livermore National Laboratory cluster at Lawrence Berkeley National Laboratory.

Author contributions

This project was conceived by N.P.B. and R.W.; N.J.S. designed and conducted the major experiments. C.F. performed the simulation study and all theoretical analysis. N.J.S., N.C.O. and E.M. performed the QENS measurements. X.Y. synthesized the PPM polymer. J.L. prepared the PPM/LiTFSI samples. H.W. guided the analysis of experimental

data. The manuscript was written by C.F., N.J.S., R.W. and N.P.B. All authors reviewed the manuscript and approved the final version. The two first authors, N.J.S. and C.F., contributed equally to this work.

Competing interests

The authors declare no competing interests.

Additional information

Supplementary information The online version contains supplementary material available at <https://doi.org/10.1038/s41563-024-01834-y>.

Correspondence and requests for materials should be addressed to Rui Wang or Nitash P. Balsara.

Peer review information *Nature Materials* thanks Bogdan Dereka and the other, anonymous, reviewer(s) for their contribution to the peer review of this work.

Reprints and permissions information is available at www.nature.com/reprints.